Eur. Phys. J. D **4**, 291–302 (1998)

THE EUROPEAN PHYSICAL JOURNAL D

Photodissociation dynamics of Cl_2 in a xenon cluster

J.M. Mestdagh[1], M. Berdah[1], N. Auby[2], C. Dedonder-Lardeux[3], C. Jouvet[3], S. Martrenchard-Barra[3], D. Solgadi[3], and J.P. Visticot[1]

[1] Service des Photons, Atomes et Molécules, CEA Saclay, 91191 Gif-sur-Yvette Cedex, France
[2] Service de Recherche sur les Surfaces et l'Irradiation de la Matière, CEA Saclay, 91191 Gif-sur-Yvette Cedex, France
[3] Laboratoire de Photophysique Moléculaire du CNRS, Bâtiment 213, Université Paris-Sud, 91405 Orsay Cedex, France

Received: 17 February 1998 / Received in final form and Accepted: 28 July 1998

Abstract. The photodissociation of a chlorine molecule in the environment of a xenon cluster has been studied experimentally using the real time pump and probe technique through the formation of an XeCl reaction product. The photodissociating system is probed in such a way that the movement of a single chlorine atom in the xenon environment is detected. Various Xe_nCl_2 cluster sizes have been investigated leading to the distinction between uncapped, half-capped and doubly capped structures for these clusters. These structures have a profound influence on the photodissociation dynamics. Retrapping of one chlorine atomic fragment and stabilization of the XeCl reaction product is only observed for the half and doubly capped clusters. The experimental work is complemented by classical molecular dynamics calculations to get a full picture of the photodissociation.

PACS. 36.40.Jn Reactivity of clusters – 36.40.Sx Diffusion and dynamics of clusters

1 Introduction

Our group has developed the Cluster Isolated Chemical Reaction (CICR) method to investigate environment effects on chemical reactions [1]. Reactants are deposited on large van der Waals clusters where they are free to migrate, to collide with each other and eventually react [2,3]. One of the phenomena observed is desorption out of the cluster of products formed on the cluster. Significant examples are given by the reaction $Ba+N_2O$ on argon clusters [4] or by the reaction between Ba_3 and SF_6 molecules [3]. Desorption of reaction products is not the only pathway, solvation within the cluster is also observed [4]. Interestingly, the branching ratio between ejection and solvation varies significantly with cluster size [5].

These observations motivate for exploring the dynamics of reaction products within cluster environments. It would be especially interesting to document the time scale of the relaxation processes that end up with product solvation or ejection. The question is addressed in the present work, both experimentally and through classical molecular dynamics simulations, by considering the photodissociation of a chlorine molecule in the environment of a xenon cluster. Reasons for this choice are recalled now.

Photodissociation is the simplest and most fundamental photochemical process. It has deserved numerous works in line with the attempt of understanding photochemistry at a microscopic level. Particular emphasis was given to photodissociation of halogen molecules in rare gas solvents, both in experimental [6–26] and theoretical [27–33] studies. A special attention was given to photodissociation of I_2 for unraveling the cage effect of the rare gas solvent that hinders the separation of the two iodine atoms [13,18–26]. Studies have been conducted along the well established real-time pump-probe technique [13,19–26], where the photodissociation dynamics is followed by Laser-Induced-Fluorescence detection of the I_2 molecule, in tuning the probe laser to a transition of I_2. These studies provide information on molecules during the dissociation and the recombination steps, but do not document the dynamics of the iodine atoms, when the I_2 molecule is fully dissociated.

Rare gas clusters can play several roles in the dissociation. The first one is the cage effect mentioned above. A second one is to trap one of the photofragments after it has left the cage where the photodissociation has taken place, into new cages where reaction products can be formed. The rare gas stands for solvent and reactant at the same time. Detecting the dynamics of a photofragment in a solvent has already appeared in the literature in a situation where one of the photofragment can react with the solvent [34,35]. For example, the ICN molecule has been photodissociated in liquid chloroalkanes, with the CN fragment doing H or Cl abstraction reactions with solvent molecules [35].

We have chosen to study Cl_2 dissociating in xenon clusters which is a simpler system where we can address the question of solvent cage exit, re-trapping and stabilization of reaction products at the most elementary level.

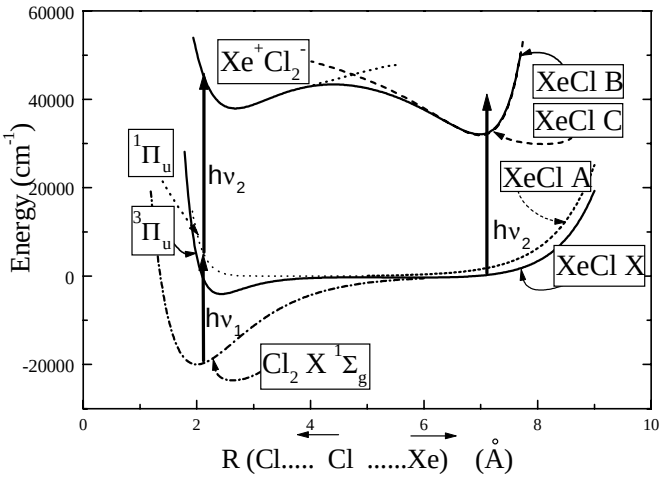

Fig. 1. Scheme of the potential energy surfaces relevant to the pump/probe experiments presented here: on the left side of the figure are presented the chlorine potential energy curves, ground state $X(^1\Sigma_g^+)$, photodissociating excited states $^{1,3}\Pi_u$ (recombination of the two chlorine atoms will take place on the $^3\Pi_u$ potential), and upper $Xe^+Cl_2^-$ charge transfer state (the Cl^+Cl^- ion pair state are not represented); on the right side are represented the XeCl potential energy curves, the ground van der Waals state X ($^2\Sigma_{1/2}$), the repulsive A ($^2\Pi_{1/2,3/2}$) state and the excited B ($^2\Sigma_{1/2}$) and C ($^2\Pi_{3/2}$) (Xe^+Cl^-) charge transfer states. In a typical experiment, the probe photon can either excite the $Xe^+Cl_2^-$ charge transfer state at short times, which will decay to XeCl B and C, or the probe photon can be absorbed by the nascent XeCl pair in its ground state to the B state, leading to fluorescence from the B and C states. The bottom axis represents a reaction coordinate of a chlorine atom moving between the other chlorine atom set at $R = 0$ and a xenon atom held at $R = 10$ Å (assuming for simplicity a linear conformation for the Cl−Cl...Xe complex)

In a sense, this work can be considered as a link between the extensive studies on the reaction of xenon with chlorine in the gas phase performed in the groups of Dubov [36–38], and Setser [39–46] and the studies in the condensed phase (liquid, matrices) in the groups of Apkarian [6–9,12,14] and Schwentner [17]. It also represents an extension of the previous work of Boivineau *et al.* [47–51] where the reactions of chlorine, bromine and iodine with xenon were investigated starting from van der Waals complexes.

In the case of chlorine in a xenon cluster, several channels are open after photodissociation: escape of the two chlorine atoms, recombinaison as Cl_2 or formation of an Xe–Cl reaction product bound by weak van der Waals forces. Among these channels, the formation of XeCl can be probed through the well-known B ← X transition at 308 nm [39,52] and the recombination channel through the excitation of Cl_2 charge transfer states around 258 nm [53,54]. A schematic view of the processes and potential energy surfaces implied in the pump-probe experiments is presented in Figure 1.

The experiment is conducted along the real-time pump-probe technique with LIF detection of the products. The pump laser dissociates the chlorine molecule within xenon clusters, at 395 nm, by exciting Cl_2 into a superposition of the dissociative $^{1,3}\Pi_u$ levels with 5000 cm^{-1} excess energy above the dissociation limit $Cl(^2P)+Cl(^2P)$ [55,56]. This is represented on the left part of Figure 1. If the chlorine atoms do not escape the cluster, different paths can be followed with different wavelengths of the probe laser and different delays between pump and probe. In the present work, two probe wavelengths have been used, 308 and 263 nm. For very short delays and with these two wavelengths, $Xe^+Cl_2^-$ charge transfer states (Fig. 1, left) can be accessed [8,14,45,47,57] which dissociate to XeCl B and C states observed through their characteristic fluorescence: the B−X fluorescence is at 308 nm and has a 10 ns lifetime while the C−A emission at 340 nm has a 130 ns lifetime [41,58] (Fig. 1, right part) and the C state is slightly lower in energy than the B state [59]. The formation and stabilization of an XeCl reaction product can be followed through the excitation of the XeCl B state with a probe laser set either at 308 nm or 263 nm and detecting the XeCl (B−X) or (C−A) fluorescence (Fig. 1, right). Finally, the recombinaison of Cl_2 can be followed through the excitation of charge transfer Cl^+Cl^- states accessible only with the 263 nm probe wavelength (not represented in Fig. 1). The excitation of these charge transfer states will most probably lead to reaction with the xenon environment to yield the final product XeCl B or C [8,14].

The experimental work is complemented by classical molecular dynamics calculations in order to clarify points that are not directly accessible to the experiment. The calculations are done with very much the same spirit than those reported by Amar and Berne for the Ar_nBr_2 system [60].

2 Experiment

The experimental setup associates a pulsed beam source, a femtosecond laser delivering the pump and probe pulses at two different colors, and a monochromator to analyze the fluorescence signal coming from the crossing zone between the cluster beam and the two laser beams.

A pulsed valve (General Valve) is used to generate the beam containing Xe_nCl_2 clusters. A gas mixture containing xenon and molecular chlorine is expanded into vacuum through a 500 μm nozzle. Three mixtures were used to generate clusters of different sizes:

$$\mathrm{He(98\%)/Xe(1\%)/Cl_2(1\%)},$$

$$\mathrm{He(80\%)/Ar(18\%)/Xe(1\%)/Cl_2(1\%)}$$

and

$$\mathrm{He(78\%)/Ar(18\%)/Xe(2\%)/Cl_2(2\%)}.$$

Stagnation pressures are typically 9 bars for the first mixture, and 5 bars for the other two. The effect of varying the stagnation pressures has been checked. In particular, the stagnation pressure has been varied between 2 and 9 bars with the second gas mixture. This has an important effect on the magnitude of the signal measured, but almost

no effect on the shape of the temporal spectra reported below. The three gas mixtures are believed to generate clusters of increasing mean sizes, ranging from small clusters with the first mixture, to large clusters with the last one. It is impossible to give quantitative information on cluster sizes at this point. The computer simulation reported below will help indicating which range of cluster sizes are probed with each of these mixtures.

The pump-probe experiment is performed 1 cm downstream the nozzle, in the free jet zone of the supersonic expansion. The two laser beams are overlapped and focused colinearly with a one meter lens in this region. They make a 90° angle with the axis of the molecular beam.

The laser used in this experiment has been described elsewhere [61]. It delivers pulses in the subpicosecond regime at a repetition rate of 20 Hz. The pump process is realized by one photon at 395 nm ($\approx$ 120 fs, $\approx$ 80 μJ/pulse) generated from the doubled output of the light coming from a Ti:sapphire regenerative amplifier. The probe photons are generated in two different ways. The 263 nm photons are generated from tripling the light of the Ti:sapphire regenerative amplifier. The temporal width of these pulses is believed to be $\approx$ 120 fs as for the doubled output of the same laser. The photon pulses at 308 nm ($\approx$ 150 fs, $\approx$ 20 μJ/pulse) are obtained by frequency doubling of 616 nm photon pulses coming from a dye laser chain after compression of the pulses. The lasers are time delayed by moving a delay line in steps of 33 fs. The absolute zero delay between the pump and the probe pulses has not been determined. The zero time shown in the experimental results below has been adjusted to match the rising edge of the signal with that of the cross-correlation function of the laser pulses expected with the above mentioned pulse widths.

The crossing region between the cluster beam and the lasers is imaged onto the entrance slit of a monochromator. Detection is performed by monitoring the fluorescence at a chosen wavelength as a function of the delay time between the pump and the probe. Signals are measured using a photomultiplier tube before being recorded on a digital oscilloscope and stored on a PC-computer. At each step of the delay line, the signal is averaged for 100 laser shots. Full scans of the delay line are averaged ten times. This experimental procedure provides us with temporal spectra where the pump-probe fluorescence signal is plotted as a function of the delay time between the pump and the probe laser. In the following, positive time delays correspond to the probe pulse coming after the pump pulse.

Changing the chirp of the lasers may change the exact shape of the temporal spectra. This has been anticipated theoretically by considering the dissociation of I_2 in solid krypton [33]. Although measurable, the effect does not affect the shape of the signal qualitatively. For this reason, no attempt has been done in the present work to monitor the chirp of the laser pulses. In addition to temporal spectra, the apparatus has also been used to record fluorescence spectra in order to characterize the clusters present in the beam, and the nature of the species that are probed in the pump-probe experiment.

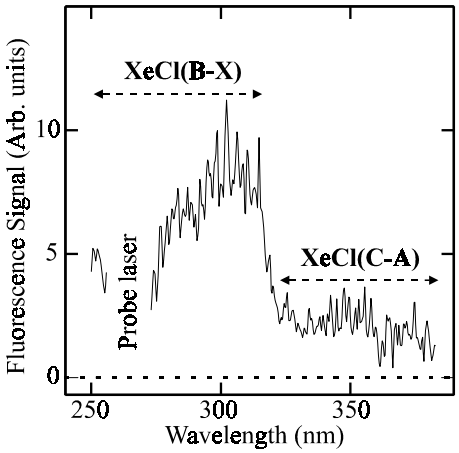

Fig. 2. Pump-probe fluorescence spectrum obtained for the couple of wavelengths 395/263 nm, for large size clusters. The fluorescence corresponding to one-laser-only excitations has been subtracted from the total fluorescence.

3 Experimental results

3.1 Fluorescence spectra

The nature of the clusters present in the beam is determined by observing the fluorescence spectrum. The spectrum shown in Figure 2 was recorded with the pump laser at 395 nm and the probe at 263 nm for a gas mixture and backing pressure corresponding to large clusters. Such spectra are obtained by subtracting the one-laser-only signals from the full signal observed when both the pump and the probe lasers are present. It has been recorded with a zero time delay between the pump and the probe lasers.

The spectrum peaks at 308 nm where the X $\leftarrow$ B emission of free XeCl exciplexes is expected [39,52]. Since collisions between particles in the beam are very scarce, observation of the Xe$-$Cl emission implies that the laser light acts on Xe_nCl_2 clusters directly, thus proving that such clusters are present in the beam. The X $\leftarrow$ B transition is energetically accessible from the two photon excitation (395 nm + 263 nm) of $Xe_{n\geq 1}-Cl_2$ complexes. The energy that is available from such an excitation is 63 000 cm^{-1}, and is comparable to that used in the work of Boivineau *et al.* to excite the Xe$-$$Cl_2$ complex with a one-color two-photon excitation [47], to that used in the VUV excitation of Xe$-$$Cl_2$ complexes [57] and to that used by Setser *et al.* to excite reactant Xe/Cl_2 pairs [40,42,45]. The shape of the emission attributed to XeCl in Figure 2, is close to that observed in reference [40], thus confirming the present assignation. The XeCl (X $\leftarrow$ B) transition is the most intense, but a red tail slightly peaking at 340 nm is observed, which is assigned to the XeCl (A $\leftarrow$ C) transition [6,39,40]. Surprisingly, the signal does not go to zero on the blue side of the probe laser ($\sim$ 250 nm). The origin of this signal will be discussed in Section 4.

A pump-probe spectrum has also been recorded with the couple of wavelengths 395 nm/308 nm. It peaks near 340 nm thus indicating that the main emitter is XeCl (C)

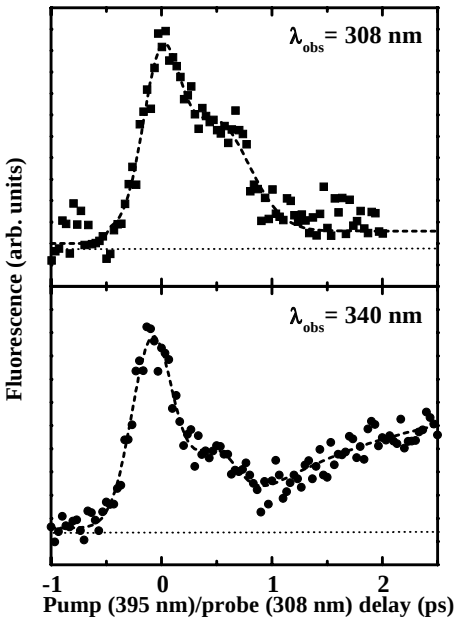

Fig. 3. Fluorescence signal as a function of the delay between pump and probe laser pulses when the system is probed at 308 nm, and the experiment run with medium sized clusters. The observation wavelengths corresponding either to XeCl (X ← B) at 308 nm or to XeCl (A ← C) at 340 nm are labeled in the figure. Positive times correspond to the probe pulse coming after the pump pulse.

when probing with 308 nm, whereas it is XeCl (B) when probing at 263 nm.

3.2 Temporal spectra

The temporal spectra observed when probing the system at 308 nm are shown in Figure 3. The experiment was conducted with medium size clusters, and observation was performed at two different wavelengths: 340 nm that corresponds to the emission XeCl (A ← C)) and 308 nm corresponding to XeCl (X ← B). The main emission is at 340 nm, and the corresponding temporal spectrum appears as a transient peak followed by a plateau. Observation at 308 nm is different since mainly the transient peak is visible. However, a plateau of very weak intensity seems to be also present. There is also a dip in the signal observable mostly for medium size clusters at 1 ps for observation at 340 nm.

Temporal spectra observed when probing the system with 263 nm are shown in Figure 4. The three classes of cluster sizes were investigated with this probe wavelength. For small clusters, only a transient peak is observed when the observation is set at 308 nm (no signal at 340 nm), whereas both the transient peak and a plateau are observed in the medium and large cluster experiments for the observation wavelengths 308 and 340 nm. The temporal spectra measured at 308 and 340 nm show no noticeable difference.

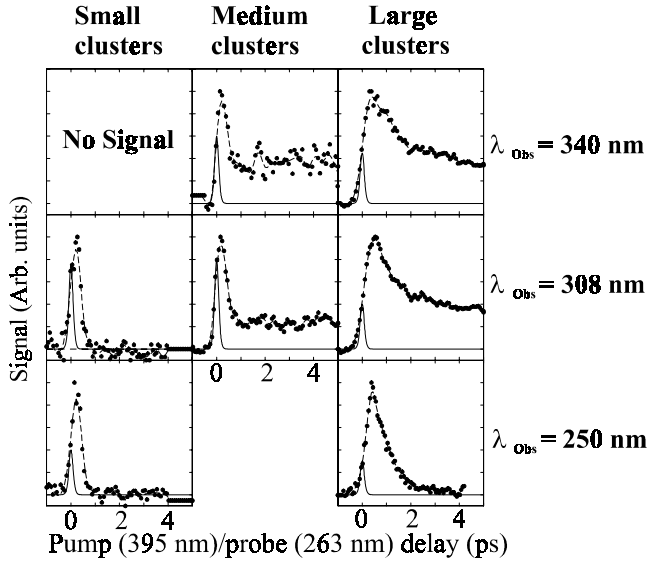

Fig. 4. Fluorescence signal as a function of the delay between pump and probe laser pulses when the system is probed at 263 nm. The observation is set at three wavelengths 250, 308 and 340 nm and three mean cluster sizes have been investigated. The full curve shows the cross correlation function of the two laser pulses.

When emission at 250 nm is monitored (for small and large clusters, no observation was done at 250 nm when running the medium size clusters), only a transient peak is observed.

4 Discussion of the experimental results

We start the discussion by considering the 308 and 340 nm emissions, characteristic of XeCl. Emission at 250 nm which may come from different excited species will be discussed later.

The 308 nm (resp. 340 nm) emission is due to XeCl(B) (resp. (XeCl(C)) exciplexes. These exciplexes have been formed in/on the cluster by absorption of a probe photon by a Xe−Cl pair, but if the exciplexes stay in interaction with the cluster, they should react with surrounding xenon atoms according to the reaction [6–8,12,17]

$$\mathrm{XeCl}^* + \mathrm{Xe} \rightarrow \mathrm{Xe_2Cl}(4^2\Gamma).$$

The fluorescence would then be that of $Xe_2Cl(4^2\Gamma)$ (localized around 490 nm in the gas phase [6] and 550 nm in a xenon matrix [6–8,17]) instead of that observed experimentally. In solid Xenon the XeCl B and C fluorescence is absent which means that the time scale for Xe_2Cl formation is less than 10 ps [6] while measurements in liquid xenon have demonstrated that Xe_2Cl is produced in 330 fs [12]. In the present case, we observe mainly XeCl (B and C), which means that either the clusters are not large enough so that XeCl escapes without interacting with other xenon atoms or the time scale for Xe_2Cl production in the cluster is much longer than in the liquid phase.

Fluorescence that could be assigned to Xe_2Cl emission ($4^2\Gamma$) has actually been observed in the present work, in the 500 nm energy region, but it was much weaker than the 308 nm fluorescence so that no pump/probe temporal studies could be performed.

The pump-probe scheme that applies for the present experiment may thus be described in the following way. The pump laser photodissociates the Cl_2 molecule, resulting in two chlorine atoms with kinetic energy. The probe laser promotes XeCl to the B exciplex state in or on the cluster. The probe wavelength 308 nm generates the B state in low vibrational levels $v \approx 0$ whereas with the 263 nm wavelength 0.7 eV excess energy is imparted to XeCl (B). The fluorescing XeCl products that are detected are those that desorb out of the remaining xenon cluster shortly after being created by the probe laser. This implies that the clusters probed in the present work are not very large, otherwise most Cl atoms would be trapped in the cluster and would not lead to the XeCl (B and C) fluorescence. Of course, the 263 nm probe makes the desorption much easier than the 308 nm probe, because of the 0.7 eV excess energy deposited into the XeCl exciplex.

Upon desorption, the XeCl exciplex either stays in the B state where it has been created by the probe laser, or is transferred to the neighboring vibronic levels of the C state. The energy transfer XeCl ($B \rightarrow C$) is indeed easily induced by collisions [6–8,43] and has been also assumed to happen in clusters [57]. We may anticipate that exciplexes which have almost no interaction with surrounding xenon atoms stay in the B state, whereas transfer to the C levels happens in the opposite case. Having this in mind, we expect that choosing the observation wavelength (308 nm or 340 nm) is a way to select XeCl exciplexes that interact more or less strongly with the xenon environment. Observation at 308 nm will mostly document exciplexes that easily leave the cluster. This happens either when the chlorine atom that is probed is already about to leave the cluster, or when the XeCl exciplex that is formed by absorption of the probe photon has a large internal energy that helps desorption. In contrast, observations at 340 nm will document situations where the chlorine atom that is probed is either substantially embedded into the xenon cluster, or has difficulties to leave the cluster because it has a very small kinetic energy.

The B to C relaxation processes can help to estimate the mean cluster size in the jet: when the probe wavelength is set at 263 nm, XeCl B state is produced with an energy of 6000 cm^{-1}; if this energy can be dissipated completely through xenon evaporation, then relaxation to the C state should be complete, XeCl C should be the main emitter. The calculated energy difference between Xe_nCl_2 and $Xe_{n-1}Cl_2$ are 700 cm^{-1} for $n = 12$ and 1000 cm^{-1} for $n = 6$ (using the model developed in Sect. 5). This indicates that the mean cluster size must be less than 10.

The above probe scheme helps rationalizing the observations of Figures 3 and 4. We start the discussion with the results of Figure 3 when the probe laser is tuned to 308 nm and the XeCl (B) exciplex is formed with almost no internal energy to help desorption. The upper panel of the figure concerns exciplexes that are both probed and observed at 308 nm. From the above probe scheme we know that such exciplexes are formed from a chlorine atom that has enough kinetic energy to escape the cluster easily, even after formation of the strong XeCl B binding, otherwise there would be electronic relaxation to the C state, lower in energy, and emission at 340 nm. This situation is encountered when detecting chlorine atoms that have not totally lost their excess energy by collisions with surrounding xenon atoms. Of course, such a situation is a transient, and the corresponding signal is expected to appear as a transient peak.

In contrast, chlorine atoms which still are on the cluster at longer times after photodissociation, can be probed at 308 nm and lead to the 340 nm emission, after the $B \rightarrow C$ energy transfer has proceeded. This phenomenon is believed to be the origin of the plateau observed in the lower panel of Figure 3.

When the system is probed at 263 nm (Fig. 4), the excited XeCl (B) exciplex has enough internal energy to desorb fairly easily out of the cluster after absorption of the probe photon. The observation done for the three classes of clusters can be rationalized in the following way.

- *Photodissociation in small clusters* yields signal at 308 nm but not at 340 nm. The absence of signal at 340 nm suggests that both chlorine atoms are close to leave the cluster when they are probed, and that the newly formed Xe−Cl reaction pair has almost no interaction with the remaining xenon cluster. This picture is consistent with the signal appearing as a transient peak only: the chlorine atoms are close enough from xenon atoms to deserve successful probes for less than 1 ps after the photodissociation pulse. At longer times, since no collision prevent them to escape the cluster, they are too far from xenon atoms to allow for the XeCl ($B \leftarrow X$) transition.
- *Photodissociation in medium size clusters.* The signal exhibits both a transient peak and a plateau, and is observable at 308 and 340 nm. This is consistent with the picture of a dissociating Cl_2 molecule hindered by surrounding xenon atoms. In this case, one of the chlorine atoms may stay trapped within the cluster, and is the origin of the plateau in the signal. Moreover, the fact that the fluorescence signal is observed both at 308 and 340 nm suggests that the XeCl exciplexes formed when probing the chlorine/xenon pair are colliding with the xenon environment when leaving the cluster.
- *Photodissociation in large clusters.* Qualitatively, the signal has the same shape than in the medium size cluster experiment. However, the transient peak is much broader. This may be viewed as a larger hindrance of the Cl_2 photodissociation by the xenon surroundings (see simulations).

We will end up the discussion by considering the emission at 250 nm, observed when probing the system at 263 nm. At first sight, the existence of this emission is puzzling since it corresponds to photons more energetic than those used to probe the system. The emission

at 250 nm may be assigned to XeCl (B) molecules that are internally excited by 0.9 eV, whereas the 263 nm excitation deposits only 0.7 eV excess energy in the molecule. Of course, the missing 0.2 eV originate from the excess energy of 5000 $cm^{-1} \approx 0.6$ eV deposited by the pump laser along the Cl−Cl dissociation coordinate. The kinetic energy of the departing chlorine atom may indeed be transformed directly as vibrational energy of the XeCl(B) exciplex upon absorption of the probe photon by an Xe/Cl pair. After accounting for the reduced mass of the Xe/Cl pair, chlorine atoms having more than 0.25 eV translational energy can account for the 250 nm emission. Such energetic chlorine atoms can only be found shortly after photodissociation, before they have lost their initial kinetic energy by collisions with surrounding xenon atoms. From this picture, emission at 250 nm is expected to appear as a transient peak in temporal spectra, and the lower panels of Figure 4 reflects the relaxation time of the kinetic energy of the chlorine atoms after photodissociation.

Direct excitation of $(Xe^+-Cl_2^-)-Xe_n$ charge transfer states which dissociate to Xe^+Cl^- in the B or C states could account for the emission at 250 nm [8,14,47,57]. With a total photon energy of 63 340 cm^{-1}, a dissociation energy of 20 000 cm^{-1} for Cl_2 there still is 43 000 cm^{-1} in the cluster. The binding energy of the exciplex Xe^+Cl^- (B or C) is 32 416 cm^{-1}, thus there is at least 10 920 cm^{-1} available to populate high vibrational levels which will emit at 250 nm [39,42]. However this process relies on direct excitation of the charge transfer states and is thus expected to follow the cross correlation function of the pump and probe lasers [14], which is not the case in the experiment. This channel is thus not the main channel leading to the 250 nm emission.

Another possibility is excitation to the chlorine Cl^+Cl^- charge transfer states among which the $D'\ ^3\Pi_g$ emits at 258 nm in the isolated molecule. These states are accessible only when the Cl−Cl bond has lengthened [53,54]: this absorption will thus appear as a transient in small clusters. If the clusters are large enough to lead to recombinaison of the 2Cl. and if the relaxation of the Cl−Cl vibration is slow, this signal should maintain at longer times, and give rise to XeCl B and C fluorescence [8].

5 Molecular dynamics simulations

5.1 Method

Classical molecular dynamics calculations are performed using the program described in [60]. The calculation allows us to solve the equations of classical dynamics and therefore, starting from a given configuration of the cluster, to follow the movement of the constituents of the cluster. The molecular dynamics calculations performed in the present work involve three different sets of potential curves, in order to follow the system before and after photodissociation. Trajectories run on the ground state surface (potential 1) enable to explore the different configurations of the clusters and as will be explained in the following to determine the equilibrium geometries. Trajectories run on the first excited states (potential 2) enable to simulate the dissociation process and the absorption of the probe photon by XeCl or Cl_2: the pump photon leads to the excited dissociating state (potential 2) where the system evolves, and the probe photon promotes the system to the final state which fluoresces (potential 3).

The potential energy surfaces used in the simulations are calculated from the addition of pair potentials describing the interaction between the individual atoms in the cluster. The parameters used to model the potentials are listed in Table 1. The chlorine molecule is treated as two chlorine atoms interacting through the proper potential,

Table 1. Expression of the atom-atom potentials (in cm^{-1}) used in the simulations as a function of the distance r(Å) between atoms.

Ground state
Xe−Xe [68] $V(r) = 4\varepsilon(\sigma^{12}/r^{12} - \sigma^6/r^6)$ with $\varepsilon = 195.6$ cm^{-1} and $\sigma = 3.88$ Å
Xe−Cl(X) [66,67] ESMSV (Exponential Spline Morse Spline Van der Waals) potential
Cl−Cl (X, $^1\Sigma_g^+$) [56,65] $V(r) = De(1 - e^{-\beta(r-re)})^2 - De$ with $De = 19\,961$, $\beta = 2.036$ and $re = 2.11$
Cl−Cl ($^3\Pi_u$) [69] $V(r) = De\left[\dfrac{1 - e^{-b(r-re)}}{1 - ce^{-b(r-re)}}\right]^2$ with $De = 3341.17$, $re = 2.43111$, $c = -0.104742$ and $b = 2.525$
Dissociative Cl_2 state
Cl−Cl ($^1\Pi_u$) [56] $V(r) = A\,e^{-\alpha r^2}$ $A = 1.9986 \times 10^6$ and $\alpha = 1.33$
Probed state
Xe−Cl (B) [66,67] ESMSV potential
$Cl-Cl^-$ [71] $V(r) = De(1 - e^{\beta(r-re)})^2 - De$ with $De = 1693.65$, $\beta = 1.21$ and $re = 3.39$
Xe^+-Xe or Cl^--Xe: ion-non polar molecule interaction $V(r) = \dfrac{e^2\alpha}{2(4\pi\varepsilon_0)^2 r^4}$ with $\alpha = 4.04 \times 10^{-24}$ cm^3 [70]

each atom being considered as spherical. No attempt is done to model the alignment and orientation dynamics of the Cl p orbitals moving in the xenon cluster. Such a treatment is beyond the scope of the present work. It has been done in the group of Gerber when investigating the dynamics of $Cl(^2P)$ and $F(^2P)$ atoms in solid rare gases [62,63] and by Gersonde and Gabriel using DIM potentials [64].

Ground state PES: potential 1

Three different pair interactions are involved in constructing this PES:

- Cl−Cl in the ground state ($^1\Sigma_g^+$) of the Cl_2 molecule modeled with a fitted Morse potential [56,65];
- Xe−Cl using the potential of XeCl (X) derived by Aquilanti *et al.* [66,67];
- Xe−Xe is a standard Lennard-Jones potential [68].

Excited dissociating PES: potential 2

In the excited state, where the trajectories are run, the Cl_2 ground state potential is replaced by the dissociative $^1\Pi_u$ state, with an exponentially decreasing potential fitted on the curves calculated by Peyerimhof and Bunker [56] while the other pair potentials (Xe−Xe and Xe−Cl) remain unchanged. Besides, the $A'^3\Pi_u$ state calculated Hua [69] has also been introduced in order to model the chorine atoms recombinaison.

Final fluorescent PES: potential 3

The final state is reached by excitation from the dissociating state [Cl_2 ($^1\Pi_u$)−Xe_n] to the XeCl B excimer states which is a charge transfer (Xe^+Cl^-) state [Xe^+Cl^-−Xe_m−Cl*]. This charge transfer character of the final state leads to introduction of more potentials:

- the XeCl B state is modeled with the potential derived by Tellinghuisen [52];
- the Xe−Xe potential remains unchanged, but the dipole-dipole induced electrostatic interaction between Xe^+Cl^- and the other xenon atoms has also been taken into account with the Xe polarizability being $\alpha = 4.04 \times 10^{-24}$ cm^3 [70];
- the Cl_2^- $^2\Pi_{g1/2}$ potential is a Morse potential derived from that described by Chen and Wentworth [71].

Construction of Xe_nCl_2 ground state isomers

The simulations are performed in the ground state potential energy surface (potential 1) where the most stable isomers are generated using the quenching method described by Amar [72]: the calculation is initiated by placing the xenon atoms in a cubic structure. The system is given an initial temperature of 160 K and evolves freely, exploring a phase space which is large enough to include the deepest and local minima of the potential surface. Periodically, the system is cooled down by adding a friction force until a minimum in the potential surface is found. The configuration of all the isomers are stored, and the most stable one is used as starting point for a photodissociation simulation.

Simulation of the pump-probe experiment

Starting from the calculated minimum configuration, a small amount of kinetic energy corresponding to a small temperature is added in the cluster (in the experiment, the clusters are not very cold) and a trajectory is run on the ground Xe_nCl_2 state. The system evolution is used to generate a series of 300 different initial configurations used as starting points for the photodissociation.

At time $t = 0$, the photodissociation of the Cl_2 molecule happens, *i.e.* the Cl−Cl interaction potential is switched from the ground state potential (potential 1) to the repulsive $^1\Pi_u$ potential (potential 2). The Cl−Cl distance increases while the Cl−Cl binding energy decreases leading eventually to the formation of an Xe−Cl pair. This Xe−Cl pair can then absorb the probe photon. This possibility is tested every 10 fs on the excited state trajectory.

Absorption of a probe photon corresponds to production of the XeCl(B) exciplex that has the electronic structure Xe^+Cl^-. The test consists in selecting successively each xenon atom and each chlorine atom of the cluster and turn them into an Xe^+Cl^- molecule. The new energy of the cluster is calculated using the excited state potential energy surface (potential 3). The energy difference between potential 2 and 3 is compared to the probe photon energy. Because the kinetic energy has to be conserved during the photon absorption (classical Franck-Condon principle), the probe photon can only be absorbed if the calculated potential energy difference is equal to the photon energy (taking the spectral width of the probe laser into account). The excitation probability by the probe photon at a given delay time between the pump and the probe signal is 0 if $(\Delta E_{pot} - h\nu)/h\nu$ is greater than 1% and $[1 - 100(\Delta E_{pot} - h\nu)/h\nu]$ if $(\Delta E_{pot} - h\nu)/h\nu$ is less than 1%.

The dynamics on potential 2 is not stopped as soon as a probe photon absorption test is successful but absorption at longer delays is tested. This is the equivalent, in the simulation, of the fact that the probe laser absorption probability is small.

Successful absorptions are stored in an histogram where the horizontal scale is the time, by step of 10 fs. The simulated temporal spectrum is obtained by summing the histograms from the 300 initial configurations that have been stored in the second step of the calculation.

This model can be improved by taking into account the possibility for the two chlorine atoms to recombine as a bound Cl_2 molecules. This question has been explored in the group of Apkarian, who showed that recombination occurs on the $A'^3\Pi_u$ potential [8]. The possibility of recombination was simulated by commuting the Cl−Cl

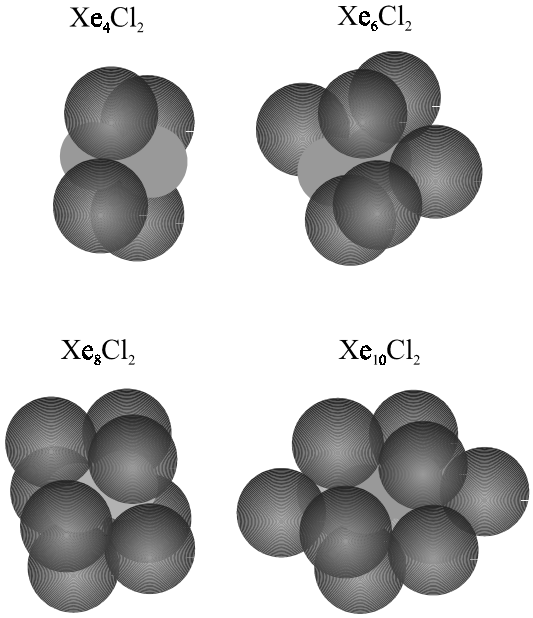

Fig. 5. Most stable configurations of four Xe_nCl_2 clusters.

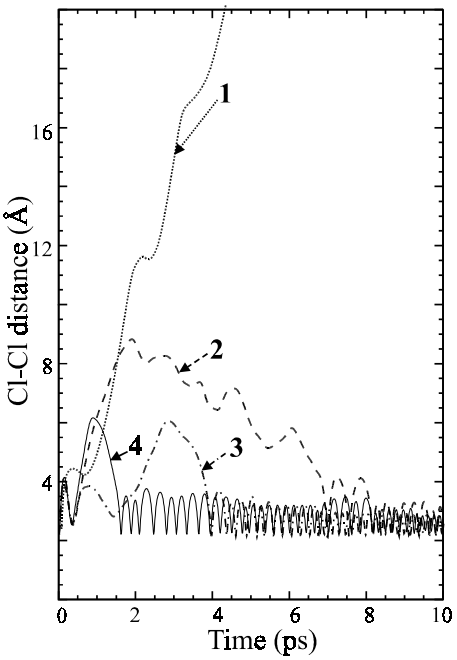

Fig. 6. Time evolution of the Cl−Cl distance after photodissociation of Cl_2 in $Xe_{11}Cl_2$ at 60 K cluster temperature. The four curves correspond to four trajectories in the simulation.

interaction in potential 2 from $^1\Pi_u$ to $A'\,^3\Pi_u$ when the Cl−Cl distance becomes larger than 4.6 Å: the potential surface change has to conserve the energy, which should in principle only be possible when the $^1\Pi_u$ and the $^3\Pi_u$ are isoenergetic, *i.e.* for at an infinite distance. But within the calculation precision, the switching can be performed for a Cl−Cl distance larger than 4.6 Å without perturbing the energy conservation.

No simulation has been done to interpret the emission observed at 250 nm after probing the system with 263 nm. Indeed, simple calculations such as those performed here do not give information on the energy of the emitted photon and cannot help to choose between the different possible mechanisms. This would need to run dynamics on several upper states coupled together and is beyond the scope of our simple calculations.

5.2 Results and discussion of the simulations

Xe_nCl_2 clusters of various sizes ranging from $n = 1$ to $n = 25$ have been constructed as explained above. Four equilibrium structures corresponding to $n = 4$, 6, 8 and 10 are shown in Figure 5. The chlorine molecule is at the center of a xenon ring for Xe_4Cl_2, and tends to be surrounded by xenon atoms in larger clusters. This reflects the greater binding energy of Xe−Cl_2 as compared to that of Xe−Xe. The structures shown in Figure 5 exhibit the three behaviors described by Amar and Berne [60] for the Ar_nBr_2 system: *uncapped*, *half-capped* and *doubly capped* structures. The difference is that six xenon atoms are enough here to observe the *half-capped* structure whereas 9 argon atoms were necessary to get the same structure for Ar_nBr_2. Similarly the *doubly capped* structure of Xe_nCl_2 is obtained with $n \geq 10$ whereas that of Ar_nBr_2 is obtained for $n \geq 17$.

Figure 6 shows the behavior of the system along the Cl−Cl coordinate for 4 different trajectories when simulating the Cl_2 photodissociation in $Xe_{11}Cl_2$ clusters at 60 K. Trajectory 1 ends up with dissociation, one of the two chlorine atoms staying trapped on the cluster. The three other trajectories lead to recombination of the chlorine atoms as a Cl_2 ($A'\,^3\Pi_u$) molecule. The corresponding time scale is very dependent on the trajectory, 2 to 7 ps in the examples reported in Figure 6. In contrast to this, the behavior of the system during the first 250 fs is very much the same, whatever the trajectory. This part of the trajectory corresponds to the first collision of the dissociating chlorine atoms with the xenon cage. The results reported in Figure 6 suggest that this first bounce is almost trajectory independent, whereas the dislocation of the cage that follows is very sensitive to the initial configuration of the cluster. Such a behavior has already been observed for the similar $Ar_{20}Br_2$ system [60].

Several final configurations of the dissociating cluster can be imagined: full dissociation with both chlorine atoms escaping the cluster, full dissociation with one of the chlorine atom staying solvated within a xenon environment (for example, trajectory 1 in Fig. 6), and finally, full dissociation but without chlorine ejection followed eventually after some time, by recombination of the two chlorine as a $Cl_2(A'\,^3\Pi_u)$ molecule. Of course, the relative occurrence of these three events should strongly depend on the cluster size as shown in Figure 7, where it appears that clusters may be separated in three classes: taking the half maximum on each curve as a class limit, the small cluster class corresponds to $Xe_{\leq 4\,\mathrm{or}\,5}$−$Cl_2$ where neither stable XeCl reaction product nor Cl_2 recombinaison

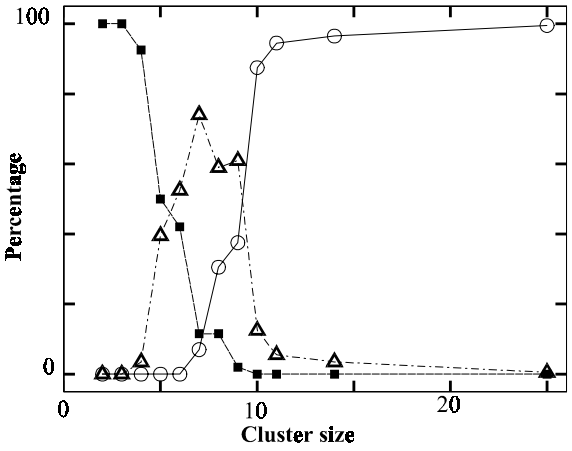

Fig. 7. Percentage of trajectories corresponding to departure of two chlorine atoms from the cluster (full squares), departure of only one chlorine atom (open triangles) and trapping of both chlorine atoms by the cluster (open circles), as a function of the cluster size. The curves are for guiding the eyes.

are observed, the medium cluster class corresponds to $Xe_{5\leq n\leq 9}Cl_2$ where only one chlorine atom stays solvated in the xenon cluster, leading to the formation of the stable XeCl reaction product. Finally, the large cluster class $Xe_{\geq 9\,\mathrm{or}\,10}Cl_2$ is when both chlorine atoms stay trapped on the cluster leading mostly to chlorine recombination. Of course, these limits should be considered as indicative. In particular, they depend on the cluster temperature. The probability of chlorine recombination decreases significantly above 60 K, to the benefit of one chlorine atom solvation. Interestingly, the classification that has just been made in terms of small, medium and large clusters, essentially matches the distinction between *uncapped*, *half-capped* and *doubly capped* calculated structures.

Temporal spectra have been simulated for various cluster sizes and various cluster temperatures. The calculated spectra have been convoluted by the temporal resolution of the experiment, *i.e.* by the cross-correlation function of the pump and the probe lasers, to make them comparable to the experimental spectra. Size effects on the temporal spectra are shown in Figure 8, temperature effects are shown in Figure 9. The results are reported for the two probe wavelengths, 263 and 308 nm, used in the experimental part of the present work. The figures show that whatever the size or the temperature of the cluster, the signal has qualitatively the same shape: a transient peak followed by a plateau. Quantitatively, the height of the plateau and the width of the transient peak depend significantly on the size and temperature of the cluster as well as on the probe wavelength.

Let us investigate size effects first (Fig. 8). Whatever the probe wavelength, 263 or 308 nm, the behavior is nearly the same. To larger cluster sizes correspond higher plateau and larger widths of the transient peak. However there is a small difference between 263 nm and 308 nm probe wavelength: at 308 nm a dip appears at $\Delta t = 1$ ps in the experimental spectra (Fig. 3) as well as in the simulation (mostly for medium size clusters Fig. 8). From the

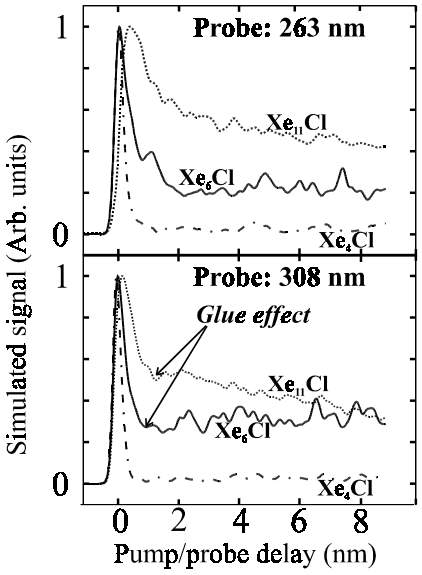

Fig. 8. Simulated temporal spectra for the two probe wavelengths labeled in the figure. Three cluster sizes are presented $Xe_{11}Cl_2$ (dots), Xe_6Cl_2 (full line) and Xe_4Cl_2 (dot-dashed). The calculation is performed for a temperature of 55 K.

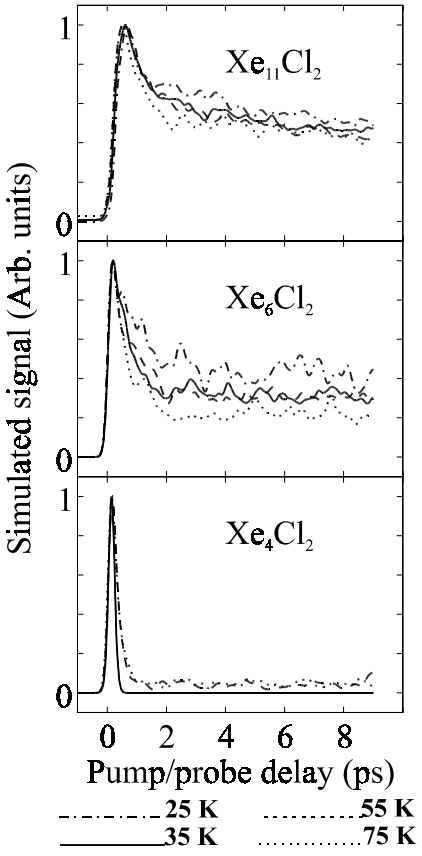

Fig. 9. Temporal spectra simulated for the three cluster sizes labeled in the figure. The probe wavelength is 263 nm. Four temperatures are investigated as indicated under the figure.

trajectories, this dip can be explained as a "glue" spring effect: a Cl atom is beginning to escape from the xenon cluster with a low kinetic energy; when this atom is far enough from xenon, no absorption can take place (dip). But long range attraction forces drive the chlorine atom back to the cluster, which leads to the plateau observed after 1 ps. At 263 nm, the Xe−Cl absorption can take place at larger distances and the dip at 1 ps is thus not observed.

The distinction between small, medium and larger cluster, or equivalently between *uncapped*, *half-capped* and *doubly capped* structures is apparent in the Figure 8. Clearly, the *uncapped* structures, *i.e.* the $Xe_{\leq 4}Cl_2$ clusters lead to narrow transient peaks, followed by a very small plateau. In this case, no, or almost no interaction exists between the two departing chlorine atoms and the xenon atoms, just because of the uncapped structure. Absorption of the probe photon is then possible only a short time after photodissociation, as anticipated in Section 4. The weak plateau implies that even for clusters as small as Xe_4Cl_2, the very weakly bound XeCl product can be stabilized despite the large kinetic energy imparted to the chorine atoms.

The Xe_6Cl_2 clusters are *half-capped* clusters. This implies that one of the two chlorine atom is not free to leave the cluster which immediately shows up as a plateau in the temporal spectrum. When switching to the *doubly capped* clusters, *i.e.* $Xe_{11}Cl_2$, the rise time of the transient peak is longer and its width is larger. Both effects are interpreted when considering the expansion of the xenon cage after the molecular chlorine photodissociation has been initiated. After the photodissociating pulse, the chlorine atoms starts to separate and shortly hit xenon atoms of the solvent cage, thus communicating translation momentum to surrounding xenon atoms, and initiating the expansion of the solvent cage. For cluster that are not totally doubly capped, this expansion results fairly rapidly into cage dislocation and one or two chlorine atoms can leave the cluster. For the larger clusters the expanding cage containing two chlorine atoms survives for up to 500 fs, giving rise to a transient peak of large width and slow rise time in the temporal spectrum.

We turn now to discussion of the temperature effect in Figure 9. A surprise arises when comparing the top panel which is representative of large clusters to the bottom one that represents small clusters: increasing the temperature in small clusters enhances the width of the transient peak, and makes a plateau apparent in the temporal spectrum, while the effect is reverse in the medium and large cluster calculations. In fact, the explanation stands from the cluster structure: in the uncapped structure, at low temperature, no xenon atom are present along or close to the Cl−Cl dissociation axis, therefore departing chlorine atoms have no interaction with xenon atoms and only a narrow transient peak is observed. When increasing the cluster temperature, because of the thermal movement of the xenon atoms and the chlorine rotation, several dissociation trajectories have to experience the presence of a xenon atom along the dissociation coordinate. The chlorine dissociation is thus no longer free. This affects the width of the transient peak and creates the small plateau. When turning to the large clusters, *i.e.* the *doubly capped clusters*, we must consider that the xenon cage is more rigid at low temperatures. As a consequence, departure of chlorine atoms out of the cluster is more difficult at a low temperature than at a higher one, this directly affects the width of the transient peak and the height of the plateau in the opposite way as that observed for small clusters.

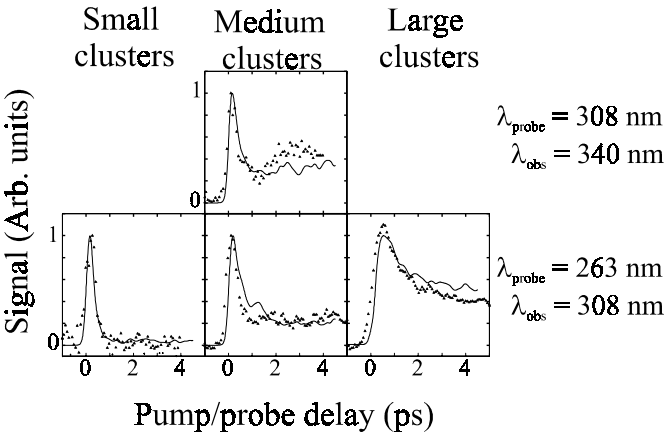

Fig. 10. Comparison between simulations (curves) and experiments (triangles). Measured and simulated temporal spectra represented in the different panels correspond to the cluster size indicated on top of each column and to probe and observation wavelengths indicated in each row.

6 Comparison between simulated and experimental spectra

Comparison between experiment and simulation is performed to test the picture of the dissociation drawn from the molecular dynamics simulations, and may further be used to estimate two main quantities not directly accessible in the present experiment: the size and temperature of the clusters. The simulated temporal spectra are compared to the most intense fluorescence emission measured experimentally, *i.e.* 308 nm when probing the system at 263 nm, and 340 nm when probing at 308 nm.

The preceding section shows that the temperature and size of the clusters have a significant effect on both the width of the transient peak and the height of the plateau in the calculated temporal spectra. It is therefore possible to use the cluster size and temperature as parameters to fit the experimental results with calculations. The criterion chosen to select meaningful comparisons is that a good agreement between calculation and experiment should not be too size selective: a good agreement for Xe_nCl_2 clusters must also be satisfactory for $Xe_{n-1}Cl_2$ and $Xe_{n+1}Cl_2$ clusters since there is a distribution of cluster sizes in the expansion. Moreover, medium size clusters have been probed at two different wavelengths (308 and 263 nm) which introduces a further constraints, since the same cluster size and

Table 2. Cluster sizes and temperature used in the simulations which are compared to the experimental results (Fig. 10).

	cluster size	temperature (Kelvin)
small clusters	$2 \leq n \leq 4$	45 ± 10
medium clusters	$5 \leq n \leq 8$	55 ± 10
large clusters	$9 \leq n \leq 12$	55 ± 10

temperature must be used to reproduce the experimental spectra corresponding to these two probe wavelengths.

Comparisons between experiments and simulations are shown in Figure 10 and the sizes and temperatures used in the calculation are given in Table 2. Although not perfect, the agreement is good: the width of the transient peaks and the height of the plateau are correctly reproduced with these simple calculations. Thus the description of the photodissociation drawn in the preceding sections seems to be corroborated by the simulations.

The cluster sizes mentioned in Table 2 when compared to the discussion of Section 5.2 indicate that the experiments run in the present work for small, medium and large clusters, actually select photodissociation in the three classes of structures found by Amar and Berne, *uncapped*, *half-capped* and *doubly capped* respectively [60].

7 Conclusion

The present work has addressed the question of chlorine photodissociation in xenon clusters and stabilization of a weakly bound reaction product. Molecular chlorine was photodissociated at 395 nm by a first 120 fs laser pulse. The Xe−Cl reaction pair was probed by detecting the fluorescence of the XeCl exciplex following XeCl (B ← X) absorption induced by the ultrashort probe laser pulse (263 or 308 nm).

The main experimental information provided by the present work are temporal spectra where the fluorescence signal is studied as a function of the delay between the pump and probe laser. The experimental data are complemented by molecular dynamics calculations and the following picture of the dissociation emerges:

- *in small clusters* containing 4 xenon atoms or less, the chlorine molecule is *uncapped* by the xenon atoms. After photodissociation, the chlorine atoms escape the cluster with almost no interaction with the xenon cluster environment. Although the dynamics mainly leads to transient signals, these very small clusters can stabilize a proportion of weakly bound Xe−Cl reaction product;
- *medium size clusters* containing between 5 and 8 xenon atoms have one end of the chlorine molecule encapped into xenon atoms, whereas the other end is free. Upon dissociation, the encapped chlorine atom has the opportunity of relaxing most of the kinetic energy that it has gained from the photodissociation. It has therefore a strong probability to stay solvated within the cage and react to give XeCl which is stabilized by the remaining xenon atoms. Of course, the cage where it was trapped prior to photodissociation is strongly dislocated;
- *in large clusters*, the chlorine molecule is fully surrounded by xenon atoms when 9 or more xenon atoms form the cluster. In that case the most probable process is Cl + Cl recombination, while detection of a reaction product is only a minor channel. The clusters that are probed in the present work are certainly not very large ($Xe_{\leq 12}Cl_2$) and the solvent cage is dislocated enough so as to allow detection of single chlorine atoms in the xenon environment.

The authors thank P. Meynadier, M. Perdrix and P. d'Oliveira who run the femtosecond source with high skill.

References

1. J.M. Mestdagh, M.A. Gaveau, C. Gée, O. Sublemontier, J.P. Visticot, Int. Rev. Phys. Chem. **16**, 215 (1997).
2. C. Gée, M.A. Gaveau, J.M. Mestdagh, M.A. Osborne, O. Sublemontier, J.P. Visticot, J. Phys. Chem. **100**, 13421 (1996).
3. C. Gée, M.A. Gaveau, O. Sublemontier, J.M. Mestdagh, J.P. Visticot, J. Chem. Phys. **107**, 4194 (1997).
4. A. Lallement, J. Cuvellier, J.M. Mestdagh, P. Meynadier, P. de Pujo, O. Sublemontier, J.P. Visticot, J. Berlande, X. Biquard, Chem. Phys. Lett. **189**, 182 (1992).
5. A. Lallement, J.M. Mestdagh, P. Meynadier, P. de Pujo, O. Sublemontier, J.P. Visticot, J. Berlande, X. Biquard, J. Cuvellier, C.G. Hickman, J. Chem. Phys. **99**, 8705 (1993).
6. M.E. Fajardo, V.A. Apkarian, J. Chem. Phys. **85**, 5660 (1986).
7. M.E. Fajardo, V.A. Apkarian, J. Chem. Phys. **89**, 4102 (1988).
8. M.E. Fajardo, R. Withnall, J. Feld, F. Okada, W. Lawrence, L. Wiedeman, V.A. Apkarian, Laser Chem. **9**, 1 (1988).
9. A.I. Katz, V.A. Apkarian, J. Phys. Chem. **94**, 6671 (1990).
10. H. Kunttu, E. Sekreta, V.A. Apkarian, J. Chem. Phys. **94**, 7819 (1991).
11. F. Okada, V.A. Apkarian, J. Chem. Phys. **94**, 133 (1991).
12. R. Zadoyan, V.A. Apkarian, Chem. Phys. Lett. **206**, 475 (1993).
13. R. Zadoyan, Z. Li, P. Ashjian, C.C. Martens, V.A. Apkarian, Chem. Phys. Lett. **218**, 504 (1994).
14. M.H. Hill, V.A. Apkarian, Chem. Phys. **105**, 4023 (1996).
15. H. Kunz, J.G. McCaffrey, R. Schriever, N. Schwentner, J. Chem. Phys. **94**, 1039 (1991).
16. J.G. McCaffrey, H. Kunz, N. Schwentner, J. Chem. Phys. **96**, 155 (1992).
17. J.G. McCaffrey, H. Kunz, N. Schwentner, J. Chem. Phys. **96**, 2825 (1992).
18. A.L. Harris, J.K. Brown, C.B. Harris, Ann. Rev. Chem. Phys. **39**, 341 (1988).
19. E.D. Potter, Q. Liu, A.H. Zewail, Chem. Phys. Lett. **200**, 605 (1992).
20. Q. Liu, J.K. Wang, A.H. Zewail, Nature **364**, 427 (1993).
21. C. Lienau, J.C. Williamson, A.H. Zewail, Chem. Phys. Lett. **213**, 289 (1993).

22. C. Lienau, A.H. Zewail, Phys. Chem. **100**, 18629 (1996).
23. A. Materny, C. Lienau, A.H. Zewail, Phys. Chem. **100**, 18650 (1996).
24. Q. Liu, C. Wan, A.H. Zewail, Phys. Chem. **100**, 18666 (1996).
25. J.M. Papaniklas, J.R. Gord, N.E. Levinger, D. Ray, V. Vorsa, W.C. Lineberger, J. Phys. Chem. **95**, 8028 (1991).
26. V. Vorsa, S. Nandi, P.J. Campagnola, M. Larsson, W.C. Lineberger, J. Chem. Phys. **106**, 1402 (1997).
27. R. Alimi, R.B. Gerber, V.A. Apkarian, J. Chem. Phys. **92**, 1551 (1990).
28. R. Alimi, V.A. Apkarian, R.B. Gerber, J. Chem. Phys. **98**, 331 (1993).
29. R.B. Gerber, A.B. McCoy, A. Garcia-Vella, Ann. Rev. Phys. Chem. **45**, 275 (1994).
30. M. Ben-Nun, R.D. Levine, Chem. Phys. **201**, 163 (1995).
31. Li Liu, Hua Guo, J. Chem. Phys. **104**, 528 (1996).
32. H. Schröder, H. Gabriel, J. Chem. Phys. **104**, 587 (1996).
33. M. Serling, R. Zadoyan, V.A. Apkarian, J. Chem. Phys. **104**, 6497 (1996).
34. E.D. Potter, J.L. Herek, S. Pedersen, Q. Liu, A.H. Zewail, Nature **355**, 66 (1992).
35. C. Wan, M. Gupta, A.H. Zewail, Chem. Phys. Lett. **256**, 279 (1996).
36. V.S. Dubov, L.I. Gudzenko, L.V. Gurvich, S.I. Iakovlenko, Chem. Phys. Lett. **45**, 330 (1977).
37. V.S. Dubov, Y.E. Lapsker, A.N. Samoilova, L.V. Gurvich, Chem. Phys. Lett. **83**, 518 (1981).
38. V.S. Dubov, Chem. Phys. **97**, 7342 (1992).
39. K. Tamagake, J.H. Kolts, D.W. Setser, J. Chem. Phys. **71**, 1264 (1979).
40. J.K. Ku, G. Inoue, D.W. Setser, J. Phys. Chem. **87**, 2989 (1983).
41. G. Inoue, K. Ku, D.W. Setser, J. Chem. Phys. **80**, 6006 (1984).
42. D.W. Setzer, J. Ku, *Photophysics and Photochemistry above 6 eV*, edited by F. Lahmani (Elsevier Science Publishers B.V., Amsterdam, 1985).
43. E. Quinones, Y.C. Yu, D.W. Setser, G. Lo, Chem. Phys. **93**, 333 (1990).
44. J. Qin, T.O. Nelson, D.W. Setser, J. Phys. Chem. **95**, 5374 (1991).
45. T.O. Nelson, D.W. Setser, J. Qin, Phys. Chem. **97**, 2585 (1993).
46. D. Zhong, D.W. Setser, Chem. Phys. Lett. **207**, 555 (1993).
47. M. Boivineau, J. Le Calvé, M.C. Castex, C. Jouvet, Chem. Phys. Lett. **130**, 208 (1986).
48. C. Jouvet, M. Boivineau, M.C. Duval, B. Soep, J. Phys. Chem. **91**, 5416 (1987).
49. M. Boivineau, J. Le Calvé, M.C. Castex, C. Jouvet. J. Chem. Phys. **84**, 4712 (1986).
50. M. Boivineau, J. Le Calvé, M.C. Castex, C. Jouvet, Chem. Phys. Lett. **128**, 528 (1986).
51. R.J. Donovan, P. Greenhill, M.A. McDonald, A.J. Yencha, W.S. Hartree, K. Johnson, C. Jouvet, A. Kvaran, J.P. Simons, Faraday discuss. Chem. Soc. **84**, 12 (1987).
52. A. Sur, A.K. Hui, J.B. Tellinghuisen, J. Mol. Spectrosc. **74**, 465 (1979).
53. J.B. Tellinghuisen, Chem. Phys. Lett. **49**, 485 (1977).
54. T. Ishiwata, A. Tokunaga, I. Tanaka, Chem. Phys. Lett. **112**, 356 (1984).
55. J.A. Coxon, J. Mol. Spectrosc. **82**, 264 (1980).
56. S.D. Peyerimhof, R. Buenker, Chem. Phys. **57**, 279 (1981).
57. C. Dedonder-Lardeux, C. Jouvet, S. Martrenchard-Barra, F. Talbot, D. Solgadi, Chem. Phys. Lett. **250**, 293 (1996).
58. P.J. Hay, T.H. Dunning Jr., J. Chem. Phys. **69**, 2209 (1978).
59. C. Jouvet, C. Lardeux-Dedonder, D. Solgadi, Chem. Phys. Lett. **156**, 569 (1989).
60. F.G. Amar, B.J. Berne, J. Phys. Chem. **88**, 6720 (1984).
61. J.M. Mestdagh, M. Berdah, I. Dimicoli, M. Mons, P. Meynadier, P. d'Oliveira, F. Piuzzi, J.P. Visticot, C. Jouvet, C. Dedonder-Lardeux, S. Martrenchard-Barra, B. Soep, D. Solgadi, J. Chem. Phys. **103**, 1013 (1995).
62. A.I. Krylov, R.B. Gerber, V.A. Apkarian, Chem. Phys. **189**, 261 (1994).
63. A.I. Krylov, R.B. Gerber, R.D. Coalson, Chem. Phys., (1996) (in press).
64. I.H. Gersonde, H. Gabriel, J. Chem. Phys. **98**, 2094 (1993).
65. K.P. Huber, G. Herzberg, *Molecular Spectra and Molecular Structure IV. Constants of Diatomic Molecules* (van Nostrand, New York, 1979).
66. V. Aquilanti, D. Cappelletti, V. Lorent, E. Luzzatti, F. Pirani, Chem. Phys. Lett. **192**, 153 (1992).
67. V. Aquilanti, D. Cappelletti, V. Lorent, E. Luzatti, F. Pirani, J. Phys. Chem. **97**, 2063 (1993).
68. W.L. Taylor, J. Chem. Phys. **64**, 3344 (1976).
69. W. Hua, Phys. Rev. A **42**, 2524 (1990).
70. T.M. Miller, B. Bederson, *Advances in Atomic and Molecular Polazabilities. A review of recent advances*, Vol. 13 (Academic Press, New York, 1977).
71. E.C.M. Chen, W.E. Wentworth, J. Phys. Chem. **89**, 4099 (1985).
72. F.G. Amar, A structural approach to the analysis of cluster dynamics, in The Chemical Physics of Atomic and Molecular Clusters, *Proceedings of the International School of Physics "Enrico Fermi"*, edited by G. Scoles (Course CVII, North Holland, Amsterdam, 1990).